PHYSICAL REVIEW E VOLUME 51, NUMBER 3 MARCH 1995

Second-order elasticity of liquid crystals within their nematic state at high frequencies

J. K. Krüger, C. Grammes, R. Jiménez, J. Schreiber,* K.-P. Bohn,
J. Baller, C. Fischer, D. Rogez,† C. Schorr, and P. Alnot‡
Experimentalphysik 10.2, Universität des Saarlandes, Postfach 151150, D-66041 Saarbücken, Germany
(Received 5 July 1994)

Within this work we present Brillouin and ultrasonic investigations performed on the liquid crystals *p*-methoxybenzylidene *p*-(*n*-butylaniline) (MBBA), *p*-azoxyanisol (PAA), 4-cyano-4-*n*-alkylbiphenyles (nCB), and 4-*n*-pentoxybenzylidene-4′-*n*-octoaniline (5O.8). Special attention has been paid to the evolution of a significant splitting of the two longitudinal polarized acoustic modes within the nematic phase. Angle-resolving Brillouin spectroscopy allowed the determination of the complete stiffness tensors and hence a discussion of the propagation of quasitransverse polarized acoustic modes in the nematic state of liquid crystals. We analyze the behavior of the eigenvectors of the relevant acoustic modes and discuss their significance for the propagation of quasishear modes. For 5O.8 we report an acoustic instability within its nematic state. We confirm the existence of a universal thermal relaxation mechanism of weak activation energy for the nematic state of classical liquid crystals. The observed hypersonic anisotropy is discussed in terms of that relaxation mechanism and is compared with that of glass-forming liquid crystals.

PACS number(s): 61.30.−v, 78.35.+c, 62.20.Dc, 64.70.Md

I. INTRODUCTION

Despite their considerable uniaxial molecular orientation, nematic classical liquid crystals (ncLC's) show no static elastic anisotropy and no shear stiffness; this is a consequence of their fluidity and their continuously broken orientational symmetry [1,2]. A characteristic property of ncLC's is the so-called flex elasticity (director elasticity) that is generally discussed in terms of the Frank elastic constants [3]. The low-frequency elastic properties, including the degeneracy of the second-order elastic properties, are well understood in the frame of existing hydrodynamic theories [2,4–6]. Slight elastic anisotropies of the order of 0.1% observed in several ncLC's with alkylic chains as end groups that were measured at ultrasonic frequencies could be explained in a satisfactory manner by intramolecular relaxation processes [5,7]. Hints for an additional relaxation process in *p*-methoxybenzylidene *p*-(*n*-butylaniline) (MBBA) at hypersonic frequencies were reported by Clark and Liao [8] and Harada and Crooker [9]. Grammes *et al.* [10] recently confirmed this hypothesis and generalized it to other ncLC systems.

In their pioneering Brillouin work, Bradberry and coworkers [11,12] showed a hypersound anisotropy of several percent for the nematic state of the 4-cyano-4-*n*-alkyloi phenyles (nCB) family. Later on, hypersonic anisotropies of the same amount were reported for 7OCB [13,14] and 8OCB [15], suggesting that a rather general mechanism is responsible for the disappearance of the elastic degeneracy in almost all ncLC's. Despite these hypersonic anisotropies for longitudinal polarized acoustic modes, no transverse modes have ever been observed.

More recently, Krüger and co-workers [13,16,17,18] related the large hypersound anisotropies of about 50% found for glass-forming side-chain polymer liquid crystals (spLC's) to their dynamic glass transition. As expected, these hypersonic anisotropies are accompanied by the appearance of two different pure shear modes.

The aim of the present work is to elucidate the behavior of second-order elasticity of ncLC's at ultrasonic and hypersonic frequencies, including the evolution of hypersound anisotropies. In order to prove that these hypersonic anisotropies reflect an almost universal property of ncLC's we report comprehensive elastic stiffness data for four different classes of ncLC's and compare them with Brillouin results found for glass-forming spLC's and a glass-forming mixture of ncLC's.

For ncLC's we confirm the existence of an additional relaxation process at hypersonic frequencies, different from the α relaxation of freezing liquids, and we discuss its relevance for the second-order elastic properties within the nematic state of classical liquid crystals (cLC's). In this context we report the relaxation behavior of several cLC's for their nematic state at ultrasonic as well as at Brillouin frequencies. Based on studies of the optoacoustic dispersion the hypersonic relaxation behavior is analyzed and compared with that of the isotropic state. In the case of 4-*n*-pentoxybenzylidene-4′-*n*-octoaniline (5O.8), we report indications for an unexpected acoustic softening of the stiffness coefficient c_{11}, mea-

*Present address: Fraunhofer-Institut für zerstörungsfreie Prüfverfahren, Krügerstr. 22, D-01326 Dresden, Germany.
†Present address: Laboratoire d'Ultrasons et de Dynamique des Fluides Complexes, Université Louis Pasteur, Strasbourg, France.
‡Present address: Laboratoire Central de Recherche (LCR), Thomson CSF, F-91404 Orsay, Cedex, France.

sured at hypersonic frequencies, on approaching the nematic–smectic-A transition point from higher temperatures. Implications of this softening for the propagation of quasitransverse polarized acoustic modes (QT modes) in cLC's will be discussed.

II. EXPERIMENT

A. Acoustic and optoacoustic investigations

The results obtained from classical Brillouin spectroscopy yield information about the temperature evolution of the elastic stiffness tensors of the cLC samples, and about hypersonic relaxation processes within the nematic as well as isotropic states. The details of the Brillouin techniques used in our laboratory are described elsewhere [13,19,20]. Therefore, only a very short introduction to the method is given. Monochromatic incident light with the wave vector $\mathbf{k}_i$ interacts with acoustic phonons. The inelastically scattered light is detected at a fixed scattering angle. Taking the given phonon wave vector $\mathbf{q}$ as an adjustable quantity, the sound velocity can be calculated from the measured frequency shift f of the scattered light. The basic relation for the determination of the elastic stiffness tensor $\mathbf{c}=\{c_{kl}\}$ with $k,l=1,2,\ldots,6$ is the Christoffel equation [6,21]

$$\det(\boldsymbol{l}\mathbf{c}\boldsymbol{l}^T-\mathbf{E}\rho[v(p,\mathbf{q})]^2)=0\ , \tag{1}$$

with

$$\boldsymbol{l}=\begin{bmatrix} l_1 & 0 & 0 & 0 & l_3 & l_2 \\ 0 & l_2 & 0 & l_3 & 0 & l_1 \\ 0 & 0 & l_3 & l_2 & l_1 & 0 \end{bmatrix}\ . \tag{2}$$

$\mathbf{c}$ is the fourth rank elastic tensor of the sample written in shortened 6×6 Voigt's notation, ρ is the mass density, and $v(p,\mathbf{q})$ is the velocity of a sound mode of polarization p that propagates with the wave vector $\mathbf{q}$. $\mathbf{E}$ is a 6×6 unit matrix. l_i $(i=1,2,3)$ are the direction cosines of $\mathbf{q}$ with respect to the coordinate axes x_i of the filmlike sample defined in Fig. 1. The x_3 axis corresponds to the unique axis of the sample having fiber symmetry. If the acoustic modes involved in the scattering process are damped, the related elastic tensor coefficients $c_{kl}^*=(c_{kl}'+ic_{kl}'')$ become complex quantities. Equation (1) strictly holds true only if $c''=0$, but it may successfully be applied in the case $c'\gg c''$. In that case the measured sound velocity $v(p,\mathbf{q})$ and the sound attenuation are related to the complex stiffness modulus [6] via

$$c'(p,\mathbf{q})\cong c(p,\mathbf{q})=\rho v^2(p,\mathbf{q})=\rho f^2(p,\mathbf{q})\Lambda^2 \tag{3a}$$

and

$$c''(p,\mathbf{q})=2\pi f(p,\mathbf{q})\eta(p,\mathbf{q})=\frac{4\pi\rho v\,\Gamma(p,\mathbf{q})}{q}\ , \tag{3b}$$

with

$$\eta(p,\mathbf{q})=\frac{4\pi\rho\Gamma(p,\mathbf{q})}{q^2}\ , \tag{3c}$$

where f and Γ gives the Brillouin frequency and linewidth, respectively [half width at half maximum (HWHM)], and ρ gives the mass density. A generalized viscosity η might be introduced by Eq. (3c). The acoustic polarization parameter p has three possible values for each wave vector $\mathbf{q}$ and, in the most general case, one quasilongitudinal and two quasitransverse polarized modes exist. For ncLC's the shear stiffness vanishes, at least at all frequencies yet realized. Provided that the sound attenuation is moderate, the acoustic properties of the isotropic and nematic phases can be described by the parameter sets $\{c_{11},(c_{44}\approx0),\eta_{11},\eta_{44}\}$ and $\{c_{11},c_{13},c_{33},(c_{44}=c_{66}\approx0),\eta_{11},\eta_{13},\eta_{33},\eta_{66},\eta_{44}\}$, respectively. Within this notation, relaxing external and internal variables which are acoustically relevant would cause complex generalized viscosities η_{ij}^*, yielding [6,21]

$$c_{kl}^*=[c_{kl}-i2\pi f(\eta_{kl}'+i\eta_{kl}'')]\ . \tag{3d}$$

The principles of the experimental setup are shown in Fig. 2(a). A thin, filmlike sample (see Fig. 1) is illuminated by a laser beam of wavelength $\lambda_0=514.5$ nm. Usually the scattered light is detected at an outer scattering angle of 90°. Appropriate beam splitting and sample arrangements allow the realization of different scattering geometries and, as a consequence, phonons can be detected with wave vectors of different directions and/or magnitudes. A five- or six-pass Fabry-Pérot Interferometer analyzes the spectral components of the scattered light.

The directly measured quantities are the frequency shift f of the Brillouin line and its linewidth Γ (HWHM) at a fixed phonon wave vector $\mathbf{q}$ given by the chosen scattering geometry.

The 90A and 90R scattering geometries [13,16,19] [Fig. 2(b)] are of particular interest for Brillouin investigations on thin oriented cLC films. These two scattering geometries are easy to adjust and are complementary in order to yield the complete stiffness tensor of ncLC's with their inherent fiber symmetry (space group $D_{2h\infty}$). Using exclusively the 90A scattering geometry and turning the filmlike samples around an axis normal to its surface, a sound velocity curve can be measured as a function of the rotation angle φ ($\varphi=0$ for $\mathbf{q}\|x_3$), from which, by means of a nonlinear least squares fit, all coefficients of the real part of the stiffness tensor can be calculated.

Beyond the classical acoustic data, simultaneous measurements using the 90A and 90R scattering techniques [Fig. 2(b)] yield additional information about the acoustic

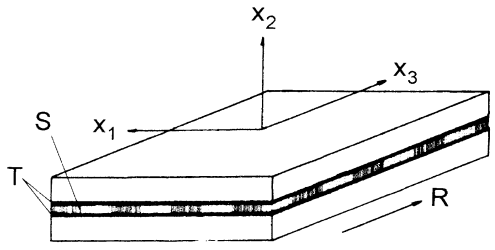

FIG. 1. Sandwich sample holder. The figure also contains the sample coordinate system (x_1,x_2,x_3). R: rubbing direction; T: PIM or PIA coated inner sides of the glass plates; S: sample material.

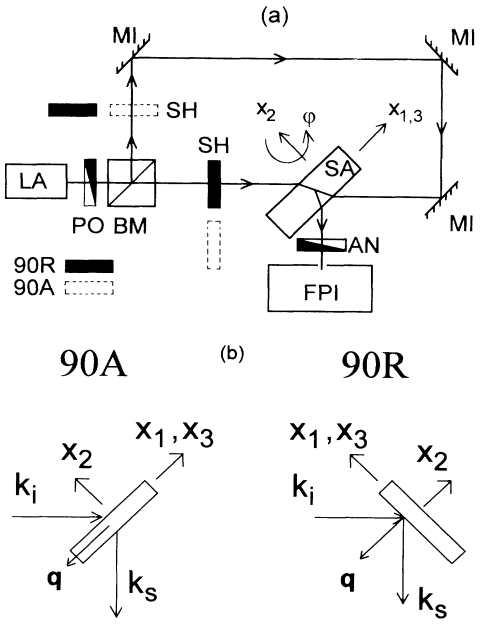

FIG. 2. (a) Schematic setup of the Brillouin spectrometer. LA: argon ion laser; BM: beam splitter; PO: polarizer; AN: polarization analyzer; SH: shutter to select light path in order to realize 90A and 90R scattering geometries; SA: filmlike sample; MI: mirror; FPI: Fabry-Pérot interferometer and detection unit; x_1,x_2,x_3: sample coordinate system; φ: rotation angle (rotation axis $\|x_2$). (b) Principles of the scattering geometries 90A and 90R. $\mathbf{k}_i$ and $\mathbf{k}_s$ correspond to the direction of the incident and scattered light's wave vector (both outside the sample); $\mathbf{q}$ is the direction of the phonon wave vector. The outer scattering angle is determined by the angle between $\mathbf{k}_i$ and $\mathbf{k}_s$; x_1,x_2,x_3: sample coordinate system.

dispersion behavior, the optical birefringence, and possibly the refractive indices of cLC's. This latter information is given by the so-called optoacoustic dispersion function (D function) [13,16,19], and is based on sound frequencies measured in the 90A and 90R scattering geometries that have been adjusted for symmetry equivalent phonon wave vectors.

For the following discussion, we define only those D_i^{90R} functions which, based on the propagation of longitudinal polarized sound modes along the x_1 and x_2 directions ($c_{11}=c_{22}$), are the most suitable for the study of optoacoustic properties of cLC's:

$$D_i^{90R}|_{c_{11}} = \left[\frac{c'^{90R}_{11}}{c'^{90A}_{11}}(n_i^2-0.5)+0.5 \right]^{1/2}, \quad (4)$$

where n_i ($i=1,3$) are the main refractive indices of the cLC sample. In the case that the acoustic dispersion can be neglected, i.e. $n_i = D_i^{90R}|_{c_{11}}$, these parameters can be evaluated from the measured hypersonic frequencies (see Sec. III).

If the hypersonic velocity depends on the magnitude of the wave vector $\mathbf{q}$, the difference $\Delta_i=(D_i^{90R}|_{c_{11}}-n_i)$ is a sensitive measure for the dispersion process involved. For hypersonic relaxation processes, $\Delta_i(T)\geq 0$ holds [13,19]. This probe for acoustic dispersion is of special interest if (i) the phonon linewidths are difficult to measure or (ii) the temperature dependence of the sound velocity and sound attenuation is available but difficult to interpret. The latter case occurs in ncLC's [10] where the hypersonic relaxation time is distributed and the process is only weakly activated, and therefore is difficult to resolve from the temperature dependence of the attenuation and velocity data.

In order to discuss the influence of the frequency on the elastic data, we performed ultrasonic measurements. These investigations were performed at 1 MHz, using a variable-frequency resonance device. A detailed description of the method, the cell and the precautions taken in order to ensure a high degree of sample purity can be found in Ref. [22]; only essential technical details are mentioned here. By use of stationary waves in a cylindrical cavity, this method allows the absolute value of the velocity to be measured from the position of the resonance peaks of the cavity. The cell was equipped with matched 3-MHz gold-plated quartzes optically polished. The diameter of the sample ($\varnothing=38$ mm) was chosen to be larger than that of the ultrasonic beam ($\varnothing=25$ mm) in order to minimize possible parasitic effects due to the side walls. The interquartz length was 7.26 mm. This value was obtained by calibrating the cell with benzene, a test liquid of known properties. The temperature of the sample was controlled to within ± 0.01 K. The ncLC's were oriented by a magnetic field of 10 kG.

B. Samples and preparation

The cLC's considered belong to chemically different classes of cLC's. Their chemical configuration and their transition temperatures are given in Tables I(a) and I(b): *p*-methoxybenzylidene *p*-(*n*-butylaniline) (MBBA), *p*-azoxyanisol (PAA), 4-cyano-4-*n*-alkylbiphenyles (nCB), and 4-*n*-pentoxybenzylidene-4'-*n*-octoaniline (5O.8). While PAA is a highly symmetric molecule with methylic end groups, the MBBA molecule has one butylic end group that provides some flexibility. In order to investigate the influence of the length of the alkyl chains on the second-order elastic properties of ncLC's, we chose four homologues of the nCB (5CB, 6CB, 7CB, and 8CB). 5O.8 possesses alkyl chains at both ends of the molecule. As a matter of fact, we found that thin samples of 5O.8 could be temporarily damaged by the incoming focused (focal length 100 mm) laser light ($\lambda=514.5$ nm). This damage occurred only at laser powers above $P=50$ mW, and was particularly efficient in the nematic phase. The damage consisted in a destruction of the molecular orientation within the laser spot, resulting in a beam broadening similar to thermal lensing. Heating the sample up to the isotropic state, the damage disappeared. We found no hints for any irreversible defects within 5O.8 samples. In order to avoid the influence of laser light on the sample properties, we performed our Brillouin measurements on 5O.8 at $P<5$ mW. Because of this low laser power and the small sample thickness of only 30 μm, the Brillouin measurements for 5O.8 were not easy to perform.

As a low molecular weight LC-nematic system with

glass-forming properties we used the mixture MIE2 (Wedler's notation [23]) (Tables I(b) and II(b)], which shows rather strong undercooling tendencies [24]. Therefore, rather moderate cooling rates of about 3 K/min are sufficient to quench the nematic liquid to the glassy state. At heating rates of 0.1 K/min, typical for Brillouin experiments, the nematic glass starts to crystallize at about $T-T_g=20$ K. At the melting point $T_m \approx 362$ K the polycrystalline material transforms to the nematic state. This material has been described in detail by Wedler [24] and Kresse *et al.* [25]. As a further glass-forming nematic material we investigated PMA6BCN [see also Tables I(b) and II(b)]. PMA6BCN is a side-chain polymer liquid crystal with a rather short main chain which consists of about only seven monomer units. This short main chain provides a sufficiently low viscosity in order to allow surface orientation. Concerning the glass transition behavior, PMA6BCN behaves similarly to an atactic polymer: a crystalline reference phase has never been observed. As a consequence, even at extremely slow cooling rates of 0.001 K/min, PMA6BCN transforms from the nematic to the glassy state and vice versa.

TABLE I. Chemical formulas of the investigated LC samples.

(a) cLC

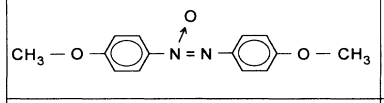	PAA
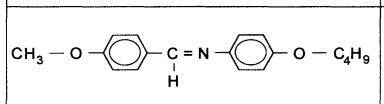	MBBA
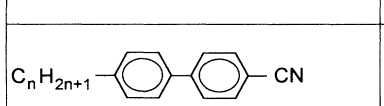	nCB
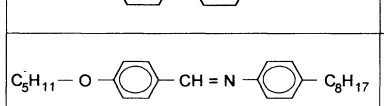	5O.8

(b) Glass-forming LC

MIE2 is a cLC mixture which consists of 70% (1), 9% (2), 12% (3), and 9% (4) (see text).

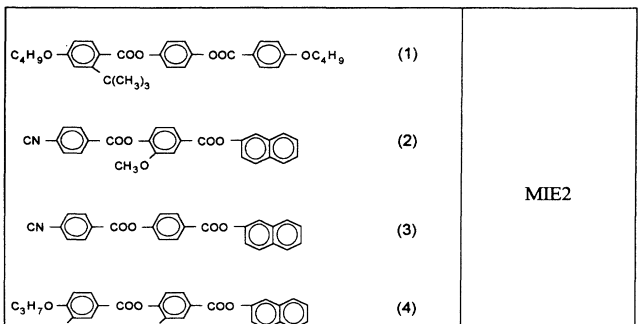	MIE2
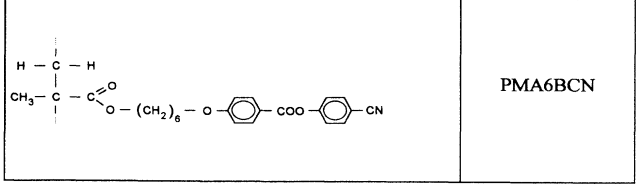	PMA6BCN

All samples for the Brillouin investigations were prepared as thin films of a thickness of about 30 μm. They were oriented by two different surface treatment techniques. We used orienting surfaces consisting of rubbed polyimide films (PIM films) as well as so-called polymer induced alignment films (PIA films). The powerful PIA technique was recently introduced by Wittmann and Smith [26]. This technique uses the fact that linear polymer and oligomer molecules tend to align themselves with their molecular chain axes on crystalline polytetrafluoro-ethylene (PTFE) along the unique axis of the PTFE layer. Because of its efficient alignment, influence on linear polymers, and related materials [26,28], we denote such a supporting PTFE film as a PIA substrate. Both the PIM and the PIA techniques yield transparent and highly oriented cLC samples perfectly adapted to Brillouin investigations. A schematic drawing of a sandwich cell including an orthogonal sample coordinate system (x_1,x_2,x_3) is given in Fig. 1. The x_3 direction has been chosen to be directed along the unique axis R of the PIM and PIA films; x_3 therefore defines the unique axis of the cLC samples, and x_2 has been defined to be orthogonal to the film plane.

In order to demonstrate the efficiency of the 90A technique in connection with the PIA preparation technique for cLC's, and to compare the results with those obtained from PIM films, we performed angle-resolving measurements [19] on 5CB and 6CB within their nematic phases. From Fig. 3 it turns out that both materials show a significant elastic anisotropy at hypersonic frequencies, and that both preparation methods yield identical stiffness coefficients within the margin of error. As a matter of fact, we usually obtained better overall homogeneity of the PIA films compared to that of the PIM films, as can be seen rather clearly in the case of 5CB.

III. RESULTS AND DISCUSSION

A. On the acoustic anisotropy of cLC's

Despite the pronounced optical anisotropy of classical nematics, there is no anisotropy observed for the static second-order elastic stiffness constants at low frequencies [1,2,4], and the shear stiffness is zero. Although both the static order parameter and the elastic strain are represented by tensors of second order, a coupling between these quantities is not observed. In general, this elastic degeneracy exists even at ultrasonic frequencies [6,29], although the relevant transport properties, represented by the viscosity tensor and the thermal conductivity tensor, reflect the fiber symmetry of the nematic state. However, there are some materials in which a small elastic stiffness anisotropy of far less than 1% has been observed [30]. This very small elastic anisotropy at

TABLE II. Phase sequences and transition temperatures (K) of the investigated samples. Phases: g, glass; cryst., crystalline; S_B, smectic(B); S_A, smectic(A); n, nematic; iso, isotropic.

(a) cLC

Phase sequence, transition temperatures in (K)

PAA	cryst.					391.2	n	408.7	iso
MBBA	cryst.					294.2	n	318.2	iso
5CB	cryst.					297.2	n	308.7	iso
6CB	cryst.					287.7	n	302.2	iso
7CB	cryst.					303.2	n	316	iso
8CB	cryst.			294.7	S_A	306.7	n	313.7	iso
5O.8	cryst.	≈ 300	S_B	322	S_A	335	n	343	iso

(b) Glass-forming LC

For MIE2 the transition temperatures of the quenched and the thermodynamic stable system are given.

MIE2 quenched system	g	285	n	387	iso
MIE2 stable phases	cryst	362	n	387	iso
PMA6BCN	g	274	n	330	iso

ultrasonic frequencies was attributed by Jähnig [31] to the freezing of trans-gauche relaxation in the alkylic end groups (e.g., Ref. [32]). As expected, this relaxation process is more evident in the related sound attenuation data [7,31].

From the innovative Brillouin work of Bradberry and co-workers [11,12] on the nematic state of the nCB family, it turned out that at least these species of liquid crystals showed a pronounced hypersound anisotropy, $(c_{33}-c_{11})/c_{33} \neq 0$, of several percent. Later on, hypersonic anisotropies of the same amount were found for 7OCB [13,14] and 8OCB [15], suggesting that a rather general mechanism is responsible for the disappearance of the elastic degeneracy in virtually all ncLC's. Therefore, it seemed of great interest to us to investigate systematically the hypersonic anomalies of different ncLC classes and to elucidate the underlying mechanism that causes their universal hypersound properties. Closely related to the question of the origin of longitudinal elastic anisotropies is the open question about the propagation of QT modes in nematic LC's.

Figures 4–6 show representative Brillouin data for nCB ($n=5$, 6, and 8). The assumption $[c_{11},c_{33},c_{13}] \gg [c_{44}=c_{55}=c_{66}(\approx 0)]$ enabled us to determine the temperature dependence of the complete elastic stiffness tensors for 5CB as well as 6CB. The elastic moduli c_{kl}, the principal sound velocities v_i, and the related attenuation coefficients Γ_i show a smooth temperature behavior in the isotropic as well as in nematic phases, and a clear splitting within the latter. The moduli c_{11} and c_{13} are close to each other. In Fig. 4 and Fig. 6 we compare our own Brillouin data with those taken from Bradberry and Clarke [12]. Although the phase

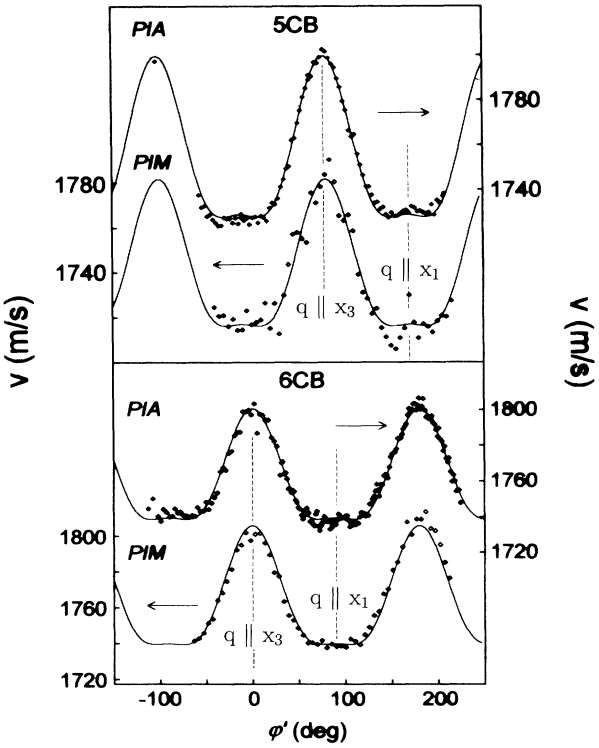

FIG. 3. Comparative angular dependent measurements of the sound velocities in 5CB and 6CB. In both cases a PIA prepared sample and a PIM prepared sample were investigated. The origin of the angle scale φ' is arbitrary and not the same for all samples. Sound propagation of the pure longitudinal modes is indicated by $\mathbf{q} \| x_3$ and $\mathbf{q} \| x_1$.

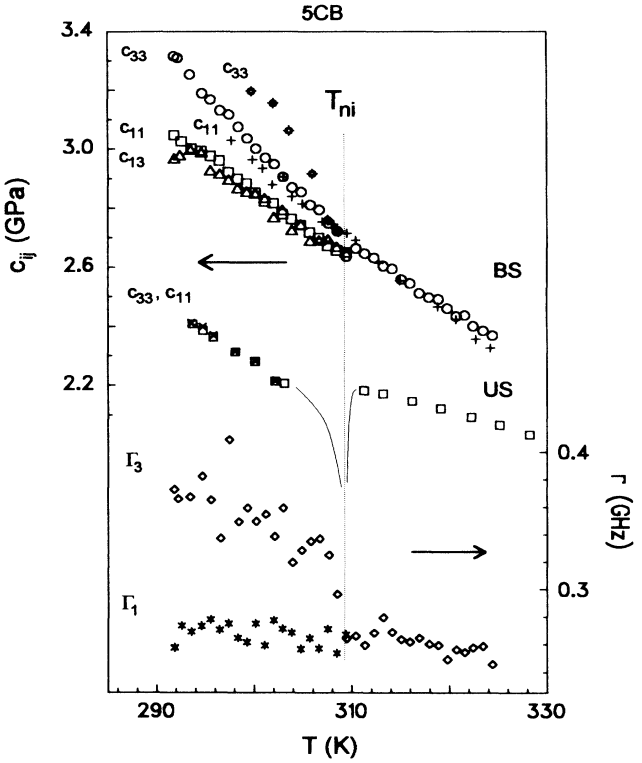

FIG. 4. Brillouin spectroscopy (BS): Elastic moduli c_{33}, c_{11}, and c_{13} (○, □, and △) and hypersonic linewidths Γ_3 and Γ_1 (◇, ★) of 5CB as functions of temperature T (our own measurements); ⊕, +: elastic moduli taken from Ref. [12] (with permission of Elsevier). Ultrasonic measurements (US): □: c_{11}; ×: c_{33} from our own measurements; T_{ni}: nematic-isotropic phase transition temperature.

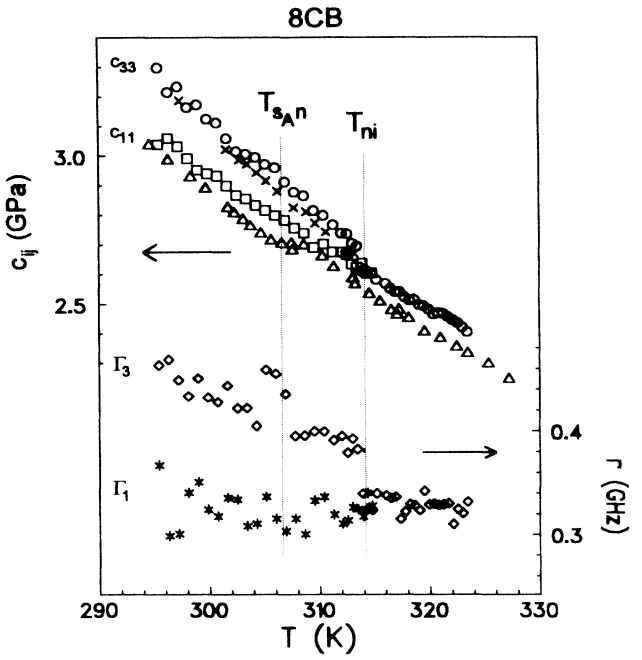

FIG. 6. Elastic moduli c_{33} and c_{11} and hypersonic attenuation Γ_3 and Γ_1 of 8CB as functions of temperature T. ○, □, ◇, ★: elastic moduli and hypersonic linewidths as measured by our group (BS); ×, △: elastic moduli measured by BS taken from Ref. [12] (with permission of Elsevier); T_{sAn}: smectic(A)–nematic phase transition temperature; T_{ni}: nematic-isotropic phase transition temperature.

transition temperatures reflected in both data sets are in rather good agreement, especially for 8CB, systematical deviations exist between the elastic data of both work groups which significantly exceed at least the margin of error of our data.

Figure 7 shows, for several ncLC's, the temperature evolution of their relative sound velocities, $\Delta v/v=(v_3-v_1)/v_1$, within their nematic state. The

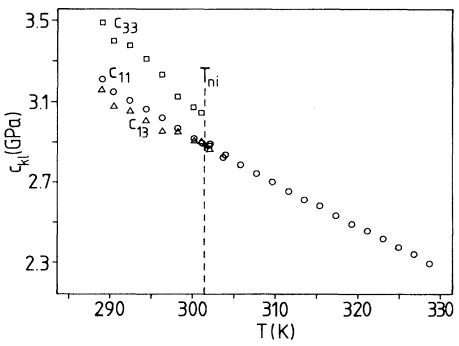

FIG. 5. Elastic moduli c_{33}, c_{11}, and c_{13} of 6CB as functions of temperature T as measured by BS. T_{ni}: nematic-isotropic phase transition temperature. □: c_{33}; ○: c_{11}; △: c_{13}.

first-order character of the nematic-isotropic transition is reflected by the steplike onset of $\Delta v/v$ at T_{ni}. It appears that $c_{33}>c_{11}$ always holds and that $c_{33}-c_{11}$ is nearly the same for all materials at the same reference temperature $T_{ni}-T$. This indicates that a rather universal mechanism is responsible for the hypersonic anisotropy. Except for PAA, the $\Delta v/v(T)$ curves for all ncLC's are bent and tend to saturate at lower temperatures, indicating a coupling between the coefficients of the elastic deformation ε_3 (Voigt notation) and the magnitude of the nematic order parameter [33] $S=\frac{1}{2}\langle 3\cos^2\theta-1\rangle$ which is only observable at very high frequencies (θ is the angle between a molecule's long axis and the director **n**).

For 8CB (Fig. 6) as well as for 5O.8 (Fig. 8), we extended our investigations to the adjacent smectic phases. The pronounced increase of $c_{11}(T)$ at the nematic–smectic-A transition temperature T_{sAn} observed by Bradberry and Clarke [12] could not be confirmed by us. In contrast to the smooth elastic behavior of 8CB, 5O.8 shows some elastic peculiarities in the vicinity of the nematic–smectic-A transition and, to some extent, does not follow the universal elastic behavior of other ncLC classes (MBBA, PAA, nCB, and nOCB [13,15]) discussed above. The most striking feature is a slowing down of $c_{11}(T)$ just above the nematic–smectic-A transition temperature T_{sAn} (Fig. 8). The corresponding preliminary results will be discussed below.

As mentioned above, in contrast to Brillouin measure-

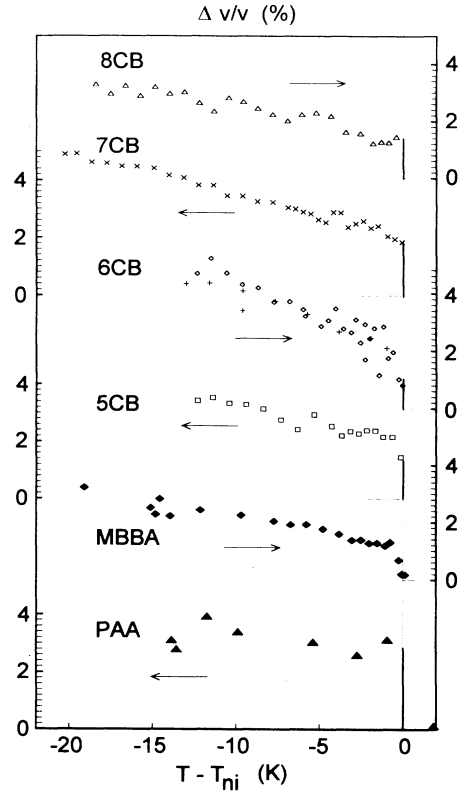

FIG. 7. Relative sound velocities $\Delta v/v=(v_3-v_1)/v_1$ of several liquid crystalline systems below the nematic-isotropic phase transition temperature T_{ni}. △: 8CB; ×: 7CB; ◇, +: 6CB; □: 5CB; ◆: MBBA; ▲: PAA.

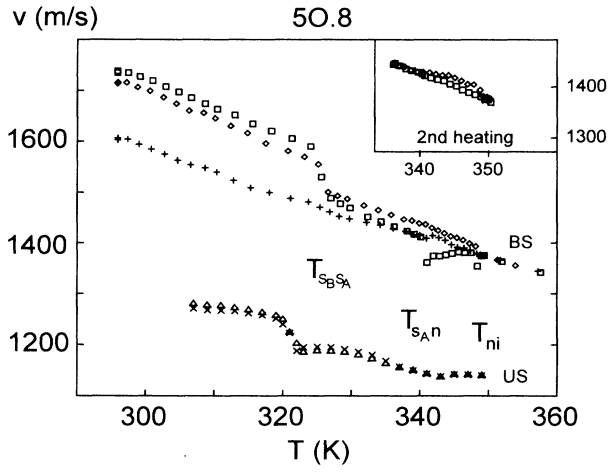

FIG. 8. Temperature dependence of the sound velocities in 5O.8. The figure contains BS measurements of our group as well as US data from Ref. [34]. The BS measurements were performed for three different directions of phonon propagation: parallel (◇), perpendicular (□), and under 45° (+) to the director **n** on heating. The inset in the upper right corner shows the behavior of v_3 (◇) and v_1 (□) after cooling below T_{s_An} during a second heating run. US data are available for **q** parallel to **n** (×), and for **q** perpendicular to **n** (△).

ments, ultrasonic measurements on the nematic phase, that have been performed at moderate frequencies (~1 MHz), show no sound velocity anisotropies within the margin of error (e.g., Refs. 6 and 10). In Figs. 4 and 8 we compare ultrasonic and hypersonic investigations made for 5CB and 5O.8 [34]. In the vicinity of the nematic-isotropic transition temperature T_{ni} of 5CB, due to the coupling between the order parameter fluctuations and the elastic strain, both longitudinal polarized sound modes tend to slow down in exactly the same manner, while the ultrasonic attenuation tends to diverge (not shown). For MBBA, Eden, Garland, and Williamson [35] have shown that the order parameter fluctuations are clamped already at 23 MHz. In accordance with this result, the longitudinal hypersonic modes of all ncLC's investigated by us (Figs. 4–7 and Ref. [10]) show no critical slowing down at all in the vicinity of T_{ni}. This means that with respect to the nematic order parameter fluctuations the Brillouin measurements are usually performed in the slow motion regime.

Moreover, Fig. 7 gives no hint of any systematic influence of the number of carbon atoms within the alkyl end groups of nCB on the hypersonic anisotropy. Although the PAA molecule contains no alkyl chains, the hypersonic properties of this material, including the elastic anisotropy, resemble that of other ncLC's (see also Ref. [10]). A structural relaxation process within the alkyl chains can therefore also be excluded as a cause for the hypersonic anisotropy.

Two further possible relaxation mechanisms, active between ultrasonic and hypersonic frequencies, should be discussed: (i) a relaxing volume viscosity η_v, and (ii) a dynamic glass transition (α process).

(i) It seems unlikely that chemically very different ncLC classes always show their main relaxation frequencies in the same small frequency regime between typical ultrasonic and hypersonic frequencies.

(ii) As a matter of fact, the static as well as dynamic glass transition temperatures (for a given frequency) depend strongly on the chemical composition of the glass former; this fact is not in line with our experimental observations. However, to make sure that a dynamic glass transition is not responsible for the observed elastic anisotropies in ncLC's, we investigated the hypersonic properties of true glass-forming nematics like spLC's (Fig. 9 and Refs. [13], [16], [17], and [18]) and a special mixture of ncLC's [*MIE*2, Figs. 10(a) and (b)]. These materials show, in contrast to what has been observed for ncLC's, very large sound velocity anisotropies of their L modes for temperatures below T_{ni}. *MIE*2 close to T_{ni} shows an anisotropy of $(v_3-v_1)/v_1\approx 6\%$, which increases at T_g to a value of 32%. For spLC's $(v_3-v_1)/v_1\approx 20\%$ is found at about $T_{ni}-T=-10$ K and increases to a value of about 50% at T_g. This strong increase of the acoustic anisotropy is due mainly to the strong increase of $c_{33}(T)$ with decreasing temperature. In contrast to the saturation behavior of the magnitude of the order parameter [16] with temperature, $c_{33}(T)$ shows even a flex point between T_{ni} and T_g. Moreover, it is interesting to note that true glass-forming nematics show a pure T phonon above the dynamic glass transi-

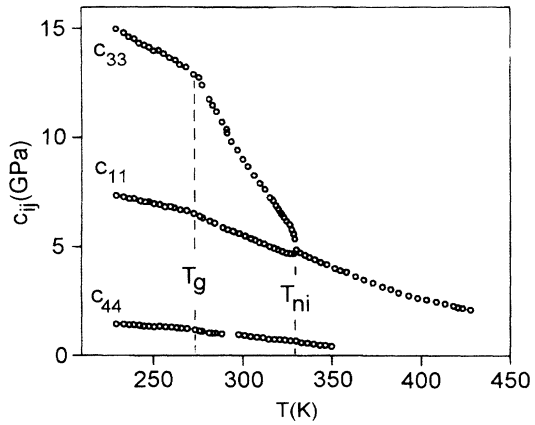

FIG. 9. Temperature behavior of the elastic constants c_{11}, c_{33}, and c_{44} of a PMA6BCN sample on heating. The static glass transition and the nematic-isotropic transition occur at $T_g = 274$ K and $T_{ni} = 330$ K, respectively.

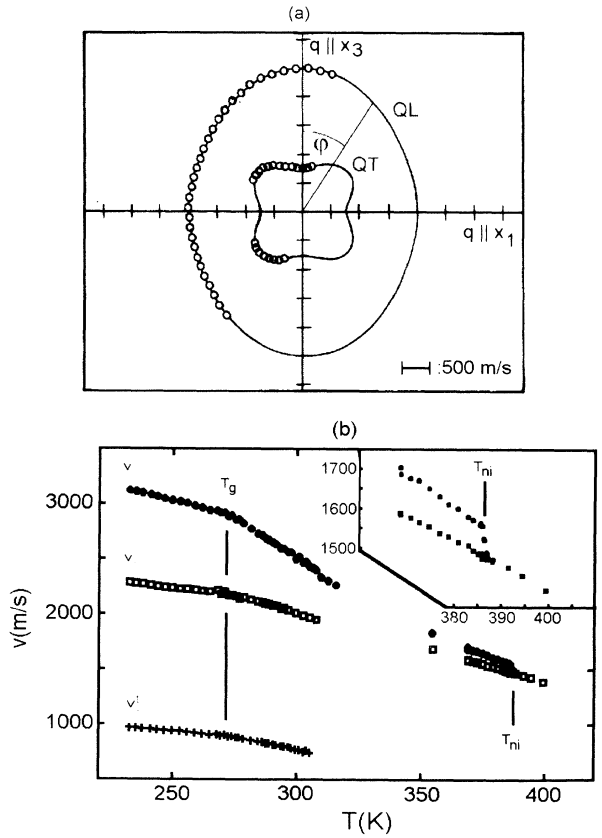

FIG. 10. (a) Sound velocity polar diagram of MIE2 at 297 K. φ is the angle between the wave vector **q** and the unique axis (x_3). QL and QT correspond to the quasilongitudinal and quasitransverse branches. (b) Temperature dependence of the sound velocity of MIE2. v_1^l and v_3^l represent longitudinal acoustic modes parallel to the unique axis (v_3^l) and perperdicular to it (v_1^l). v_3^t represents the transverse acoustic mode parallel to the director direction. T_g and T_{ni} are the static glass transition and the nematic-isotropic transition temperatures. The inset shows a temperature range around the nematic-isotropic transition.

tion. For PMA6BCN this shear mode could even be followed up to the isotropic state, until $T - T_g \approx 100$ K. As a matter of fact, neither QT modes nor T modes have ever been observed in ncLC's (see below).

Nevertheless some relaxation process must be responsible for the significant differences between the ultrasound and hypersound velocities as well as for the elastic anisotropies observed at hypersonic frequencies. Unfortunately, the flat temperature dependence of the hypersonic data (Figs. 4–6) gives no evidence by itself of the presence of any hypersonic relaxation process. This holds true for the hypersonic elastic and related attenuation coefficients, and is in contrast to observations made in glass-forming spLC's [17].

Generally, for nematic as well as isotropic states of cLC's, the ultrasound velocities $v_{US}(T)$ are systematically lower than the hypersonic ones (Figs. 4 and 8). For the isotropic state of cLC's this behavior has been attributed to the existence of a longitudinal acoustic (thermal) relaxation process that is caused by vibrational degrees of freedom within the phenyl groups of the mesogenic molecules, and which becomes macroscopically relevant for the hypersonic strain field [8–10]. In accordance with the unobtrusive temperature behavior of the hypersonic properties of cLC's within their isotropic phase, a weak activation energy of only 500 K has been estimated for this thermal relaxation process [8–10]. The weak activation energy of this process implies that its (main) relaxation time τ_{11}^{th} changes only slightly with temperature. Formally, this relaxation process can be taken into account by a complex longitudinal viscosity $\eta_{11}^*(\omega,T) = \eta_{11}'(\omega,T) + i\eta_{11}''(\omega,T)$ that, according to Eq. (3d), renormalizes the elastic stiffness $(c_{11}^*)^{iso}$, of the isotropic state. The main longitudinal relaxation frequency $f_{11}^{th} = 2\pi\omega_{11}^{th} = (2\pi/\tau_{11}^{th})$ has been found to vary between some hundred megahertz and a few gigahertz for all ncLC's that we investigated by Brillouin spectroscopy. In agreement with the measured Brillouin data, the influence of the thermal relaxation process on the shear viscosity η_{44} is believed to be negligible ($\omega_{44}^{th}\tau_{44}^{th} \ll 1$) at hypersonic frequencies, which means that $\eta_{44}^* \cong \eta_{44}'$ and $c_{44}' \cong 0$ (see below).

The important question appears of whether the above mentioned thermal relaxation process is also responsible for the hypersonic properties of the nematic state, i.e., for (i) the differences between ultrasonic and hypersonic velocities and (ii) the longitudinal hypersound anisotropies. In the context of this problem it should be mentioned that, because of the first-order character of the nematic-isotropic transition, the relaxation time could be modified abruptly as well as significantly and, in principle, differs for different directions of acoustic mode propagation. It would even be possible that the main relaxation frequencies f_r involved were renormalized in such a way that the Brillouin data of the nematic phase were measured in the slow motion regime with respect to this relaxation process.

B. On the hypersonic relaxation of ncLC's

In order to elucidate the hypersonic relaxational state of cLC's within their nematic phase, we investigated the

optoacoustic dispersion functions $D_i^{90R}|_{c_{11}}$ (Sec. II A) taking 5CB and 6CB as a model systems. Using the Brillouin setup of Fig. 2(a), Eq. (4) yields the optoacoustic dispersion functions D_1^{90R} and D_3^{90R}. Provided that x_1 and x_2 define symmetry equivalent directions, D_1^{90R} and D_3^{90R} can be determined from the sound frequencies $f^{90A}(\hat{\mathbf{q}}\|\hat{\mathbf{x}}_1)$ and $f_i^{90R}(\hat{\mathbf{q}}\|\hat{\mathbf{x}}_2,\hat{\mathbf{E}}\|\hat{\mathbf{x}}_i)$ with $i=1$ and 3, where $\hat{\mathbf{q}}$ is the unit vector of the acoustic wave vector and $\hat{\mathbf{E}}$ gives the polarizations of the incident as well as of the scattered light. The related hypersonic wavelengths Λ^{90A} and Λ_i^{90R} are given by

$$\Lambda^{90A}=\frac{\lambda_0}{\sqrt{2}} \tag{5a}$$

and

$$\Lambda_i^{90R}=\frac{\lambda_0}{\sqrt{4n_i^2-2}} \quad \text{with } i=1,3\ . \tag{5b}$$

Taking Eqs. (4)–(5*b*), we obtain the desired relation for $D_i^{90R}|_{c_{11}}$ which yields the main refractive indices n_i of an optically uniaxial sample only from Brillouin data, provided that acoustic dispersion effects can be neglected:

$$D_i^{90R}|_{c_{11}}=\left[\frac{1}{2}\left[\frac{f_i^{90R}(\hat{\mathbf{q}}\|\hat{\mathbf{x}}_2,\hat{\mathbf{E}}\|\hat{\mathbf{x}}_i)}{f^{90A}(\hat{\mathbf{q}}\|x_1)}\right]^2+\frac{1}{2}\right]^{1/2} \quad \text{with } i=1,3\ . \tag{6}$$

Comparing $D_i^{90R}|_{c_{11}}$ with the related refractive index n_i measured at the same temperature, we have a sensitive probe for the effect of hypersonic relaxations. The difference

$$\Delta_i(T)=\left[D_i^{90R}|_{c_{11}}(T)-n_i(T)\right] \tag{7}$$

measures the amount and the distribution of hypersonic relaxation effects. Within the slow motion ($2\pi f\tau\gg1$) and fast motion ($2\pi f\tau\ll1$) limits $D_i^{90R}|_{c_{11}}(T)=n_i(T)$ holds true, otherwise $\Delta_i(T)$ is positive.

It is interesting to note that the difference $\Delta D=D_3^{90R}-D_1^{90R}$ between the two main optoacoustic dispersion functions gives approximately the correct birefringence, even in the presence of hypersonic relaxations ($\Delta_i>0$) [19]. In Figs. 11 and 12 we compare our optoacoustic dispersion data with refractive index data for 5CB and 6CB taken from literature [36]. In the whole temperature range under investigation, the $D_i^{90R}|_{c_{11}}$ data significantly exceed the related values of the refractive indices $n_i(T)$. Since the difference $\Delta_i(T)$ is almost constant for both materials independently of the temperature, we conclude that the thermal relaxation process active in the isotropic state is also fully active in the nematic state. As a matter of fact, there is no hint of an approach of the D functions versus the n functions either in the isotropic or in nematic states. This result proves that the hypersonic relaxation process observed in the nematic phases of 5CB and 6CB also has a low transition energy and is probably identical to the thermal relaxation process believed to be active in the isotropic phase of cLC's.

At the top of Fig. 11 we show those sound frequencies which generate the optoacoustic D^{90R} data. It turns out that the influence of the symmetry breaking effect due to the order parameter on the pure second-order elastic properties, represented by the difference between the longitudinal hypersonic frequencies $f_i^{90A}(\hat{\mathbf{q}}\|\hat{\mathbf{x}}_i)$ ($i=1,3$), is rather small compared to the difference between the longitudinal frequencies $f_i^{90R}(\hat{\mathbf{q}}\|\hat{\mathbf{x}}_2,\hat{\mathbf{E}}\|\hat{\mathbf{x}}_i)$ ($i=1,3$), which reflects directly the birefringence Δn of our ncLC's and therefore the magnitude of the nematic order parameter S.

From Eq. (6) we obtain an approximate relation between ΔD and $\Delta n\propto S$:

$$\Delta n\cong n_1\frac{[f_3^{90R}(\hat{\mathbf{q}}\|\hat{\mathbf{x}}_2,\hat{\mathbf{E}}\|\hat{\mathbf{x}}_3)-f_1^{90R}(\hat{\mathbf{q}}\|\hat{\mathbf{x}}_2,\mathbf{E}\|\hat{\mathbf{x}}_1)]}{f_1^{90R}(\hat{\mathbf{q}}\|\hat{\mathbf{x}}_2,\mathbf{E}\|\hat{\mathbf{x}}_1)}\cong\Delta D\ . \tag{8}$$

Even if the hypersonic frequencies f^{90A} and f^{90R} are measured within a hypersonic relaxation regime, Eq. (8) yields an acceptable approximation for Δn. Generally, it is therefore possible to obtain simultaneously information about the second-order elastic properties as well as the order parameter from the same small information volume of about 10^{-7} cm^3. The ΔD and Δn data given in Figs. 11 and 12 are in excellent agreement with the predictions of Eq. (8) for the nematic state of 5CB and 6CB, and additionally confirm the concept of the optoacoustic dispersion functions.

C. On the propagation of quasilongitudinal and quasitransverse modes in the nematic state

Assuming that $c'_{QL}\gg c''_{QL}$ and $c'_{QT}\gg c''_{QT}$ hold true, and taking into account that ncLC's show fiber symmetry, Eq. (1) can be used to evaluate the following coupled pair of relations yielding the quasilongitudinal and quasitransverse polarized acoustic branches in polar representations (φ gives the polar angle between the acoustic wave vector $\mathbf{q}$ and the x_3 axis):

$$v_{QL_+,QT_-}(\varphi)=(2\rho)^{-1/2}\left\{c_{11}\sin^2\varphi+c_{33}\cos^2\varphi+c_{44}\pm\sqrt{[(c_{11}-c_{44})\sin^2\varphi+(c_{44}-c_{33})\cos^2\varphi]^2+(c_{13}+c_{44})^2\sin^2 2\varphi}\right\}^{1/2}\ . \tag{9a,b}$$

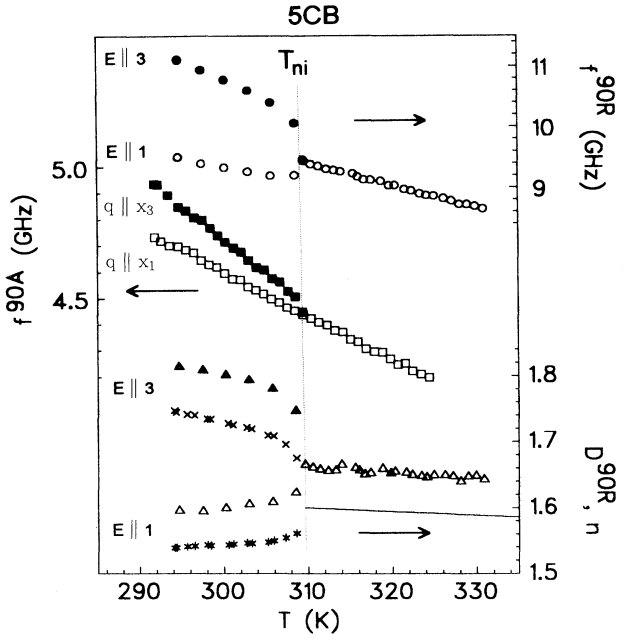

FIG. 11. Hypersonic frequencies of 5CB as function of temperature measured using the 90A and 90R scattering geometries. 90R measurement: phonon wave vector **q** along the x_2 direction, and electric polarization vector of the incident laser beam along the x_3 and x_1 directions (●,○). 90A measurement: phonon wave vector along the x_3 and x_1 directions (■,□); the direction of electric polarization vector has no influence on the result. Main refractive indices (×,★ and straight line) extrapolated from literature [36], and optoacoustic dispersion functions D_i^{90R} measured by Brillouin spectroscopy (triangles).

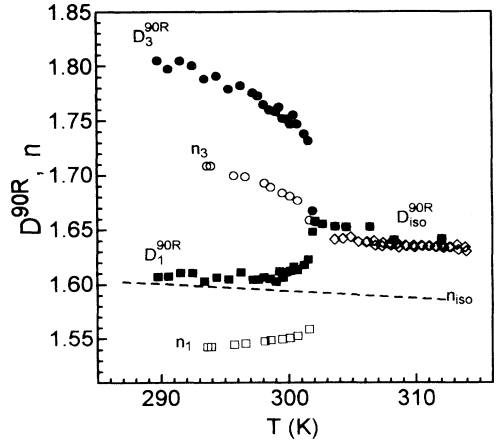

FIG. 12. Main refractive indices of 6CB (○, □, and dashed line) extrapolated from literature [36], and optoacoustic dispersion functions D_i^{90R} (filled symbols and open diamonds) measured by Brillouin spectroscopy.

Thereby v_{QL} and v_{QT} data can be used to determine c_{11}, c_{13}, c_{33}, and c_{44} by applying a least squares fit to the measured v_{QL} and v_{QT} data. Equations (9a) and (9b) are coupled, and contain some redundancy (covariance between c_{13} and c_{44}). It is not obvious how to estimate the breakdown of relations (9a) and (9b) in the case of disperse media. However, we have tested the compatibility of Eq. (9a) with Eq. (9b) successfully in the case of uniaxial viscous liquids like spLC's (Refs. [13], [16], [17], and [18]), oriented polymers [13,16], and glass-forming cLC's (MIE2, see Secs. II B and III A) well above their glass transitions [Fig. 10(a)]. We found that as long as Brillouin frequencies f_{QL} and f_{QT} can be detected, they can be treated by the Christoffel equation. Unfortunately, as far as we know, quasitransverse polarized phonons were never observed within the nematic state of classical liquid crystals, although shear phonons have been observed in glass-forming nematics (Figs. 9 and 10 and Refs. [13], [16], and [17]) and in smectic LC's (e.g., Ref. [37]). On the other hand, c_{11}, c_{13}, c_{33}, and c_{44} cannot be determined using only $v_{QL}(\varphi)$ data. This serious restriction results from the strong statistical correlation between c_{13} and c_{44} [19]. However, for ncLC's we can avoid this problem because we can make even at hypersonic frequencies the assumptions $[c_{11},c_{33},c_{13}] \gg [c_{44}=c_{55}=c_{66}\ (\approx 0)]$ for the nematic state. In that case Eqs. (9) yield the simplified relation

$$v_{QL_+,QT_-}(\varphi)=(2\rho)^{-1/2}\{A(\varphi)\pm B(\varphi)\}^{1/2}\ , \tag{10a}$$

with

$$A(\varphi)=(c_{11}\sin^2\varphi+c_{33}\cos^2\varphi) \tag{10b}$$

and

$$B(\varphi)=\sqrt{[c_{33}\cos^2\varphi-c_{11}\sin^2\varphi]^2+c_{13}^2\sin^2 2\varphi}\ . \tag{10c}$$

For $\varphi=45°$, A and B in Eq. (10) reduce to

$$\begin{aligned} A(45°)&=\tfrac{1}{2}(c_{11}+c_{33})\ , \\ B(45°)&=\tfrac{1}{2}\sqrt{[c_{33}-c_{11}]^2+4c_{13}^2}\ . \end{aligned} \tag{11}$$

As $c'_{QL} \gg c''_{QL}$ holds true, Eqs. (10) allow us to calculate the remaining stiffness coefficients from pure v_{QL} data. In the case of 5CB and 6CB we used $v_{QL}(\varphi=0°)$, $v_{QL}(\varphi=45°)$, and $v_{QL}(\varphi=90°)$ in order to determine the elastic stiffness data $\{c_{11},c_{13},c_{33}\}$ shown in Figs. 4 and 5. Using these stiffness coefficients, and in addition the temperature as a parameter, we have calculated polar plots for the QL mode [Fig. 13(a)]. Assuming the harmonic approximation to be valid, we could estimate upper limits for the QT modes [Fig. 13(b)]. Concerning the QT branch, it was not clear to us to which extent the QT phonons are underdamped at hypersonic frequencies.

Due to the small difference between c_{33} and c_{11}, the quasitransverse branches reach their maximum sound velocities at $\varphi=45°$ [Fig. 13(b)]. Therefore, if possible at all, QT modes should be resolved most easily at $\varphi=45°$. Using Eqs. (10) and (11) we estimated the quasishear sound velocity $v_{QT}(45°)$. For $T=289.1$ K we obtained $v_{QT}(45°)=311$ m/s ($\hat{=}0.9$ GHz for 90A scattering geometry). Because we did not find this phonon mode, the question appears of whether such a phonon frequency is still detectable with a classical Brillouin spectrometer. As has been shown recently [38] for transverse modes in

NaCN/NaCl mixed crystals, this phonon frequency even in the presence of significant attenuation, is still detectable with our five-pass Brillouin spectrometer, although it is close to the detection limit. Moreover, in quasismectic plastic crystals of $C_{20}F_{42}$ perfluoroalkanes we could detect quasishear frequencies at about 1 GHz even though the pure shear frequency was undetectably low [39]. Although we made great efforts in order to resolve the related quasishear phonon, we definitely had no fingerprint for the existence of a QT mode. Having excluded the spectrometer resolution as the limiting factor for the nonobservation of the quasishear Brillouin lines, two other possibilities have to be taken into account: (i) a small elasto-optical coupling, and (ii) the quasishear modes could be strongly damped.

The first hypothesis seems not to be very likely, because quasishear phonons and even shear phonons have been found in several liquid crystals at Brillouin frequencies: this holds true for the smectic-A phase and the smectic-B phase of β-methyl-butyl-p[(p-methoxybenzylidene)amino] cinnamate; for the smectic-B phase even pure transverse polarized Brillouin modes were reported [37]. As discussed above, QT and even T phonons are easily detected in spLC's and in the nematic state of the cLC mixtures, MIE2.

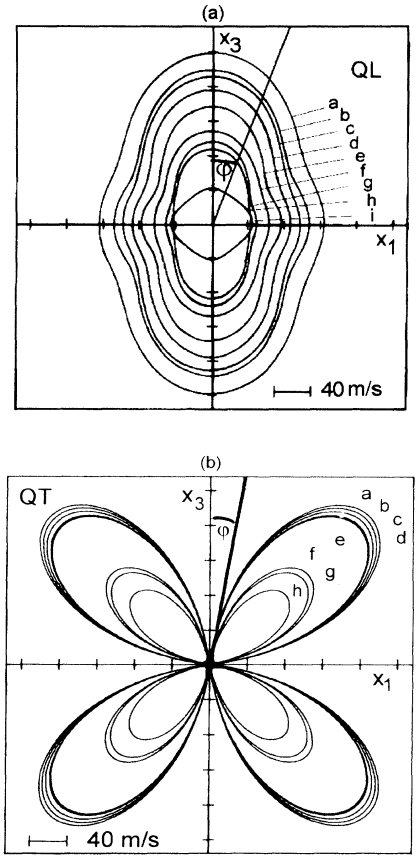

FIG 13. Sound velocity polar diagrams of 6CB at various temperatures. The curves result from nonlinear least squares fits to the data presented in Fig. 5. c_{44} has been assumed to be zero. (a) Quasilongitudinal branch. Zero point suppression of 1650 m/s. (b) Quasitransverse branch, no zero point suppression. (a) 289.1 K, (b) 290.5 K, (c) 292.5 K, (d) 294.4 K, (e) 296.4 K, (f) 298.3 K, (g) 300.2 K, (h) 301.1 K, and (i) 302.2 K.

As the pure shear modes in classical nematic LC's are almost overdamped even at hypersonic frequencies—at least they cannot be resolved—the second hypothesis is closely related to the question of the longitudinal component of the polarization vector of the v_{QT} mode. An increasing shear character of the quasishear polarization vector signifies an increasing damping of this mode. On the other hand, an increasing shear character of the QL phonon should result in an increasing Brillouin line width. The strongest influence of this effect is expected for the QL mode at $\varphi \approx 45°$. For 6CB Fig. 14 shows the φ dependence of v_{QL} and Γ_{QL} at $T \cong 295$ K. The average hypersonic attenuation is about twice that of classical organic liquids like quinoline. The attenuation curve is in phase with the sound velocity curve and there is no excessive attenuation around $\varphi = 45°$ (modulo $\pi/2$), which in turn indicates a weak deviation of the QL polarization from the pure longitudinal one.

In order to estimate the polarization of the $v_{QL}(45°)$ and $v_{QT}(45°)$ modes, we calculated the eigenvector $\mathbf{p}_{QL}^{45°}$ of the related QL(45°) phonon within the harmonic limit as a function of temperature. Because of the rather weak attenuation of the $v_{QL}(\varphi)$ mode, this procedure seems to be justified for the determination of $\mathbf{p}_{QL}^{45°}$. As a rough measure of the transverse contribution to the QL mode, we use the direction cosine between $\mathbf{p}_{QL}^{45°}$ and the unit vector of the wave vector $\mathbf{q}$ and define

$$L_q^{45°} = 1 - \hat{\mathbf{q}} \cdot \frac{\mathbf{p}_{QL}^{45°}}{|\mathbf{p}_{QL}^{45°}|} \,. \tag{12}$$

For 5CB, 6CB, and 5O.8, Fig. 15 shows that the parameters $L_q^{45°}$ are very weak and decrease as T approaches T_{ni} from below. As a consequence, $\mathbf{p}_{QT}^{45°}$ becomes almost T polarized. Therefore, we conclude that the v_{QT} modes

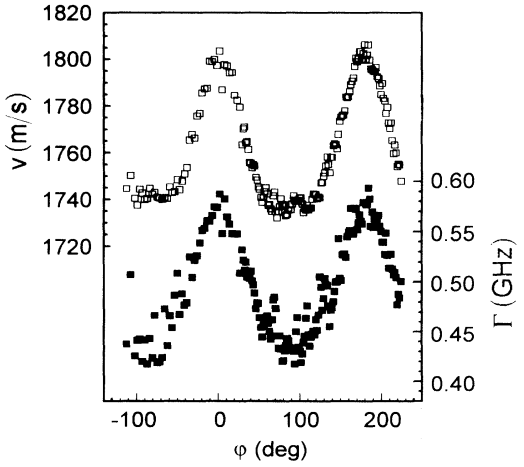

FIG. 14. Angular dependence of the sound velocity v_{QL} within the x_1-x_3 plane and the corresponding BS linewidth Γ_{QL} of 6CB at $T \cong 295$ K.

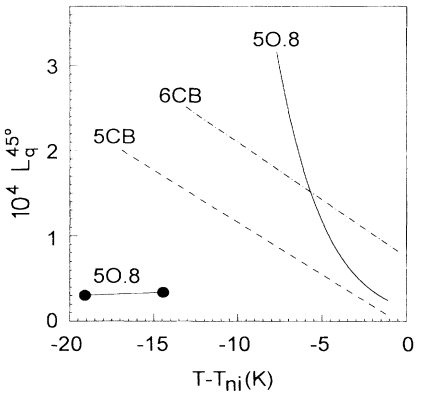

FIG. 15. Temperature dependence of the parameter $L_q^{45°}$ below the nematic-isotropic phase transition (T_{ni}) for 5O.8, 6CB, and 5CB (for further information, see text).

cannot be observed because they are extremely attenuated even at hypersonic frequencies.

D. On the peculiarities at the nematic-smectic phase transition

As mentioned above, a somewhat peculiar hypersonic behavior is found for the nematic state of 5O.8 (Fig. 8). Once again we have measured $v_{QL}(\varphi=0°)$, $v_{QL}(\varphi=45°)$ and $v_{QL}(\varphi=90°)$ as a function of temperature. At T_{ni} $v_{QL}(\varphi=45°)$ and $v_1=v_{QL}(\varphi=90°)$ behave nearly continuously, whereas $v_3=v_{QL}(\varphi=0°)$ performs a small positive step. On approaching the nematic–smectic-A transition from below, $v_1=v_{QL}(\varphi=90°)$ shows a slowing down which is accompanied by a small maximum of the hypersonic attenuation Γ_3 just above T_{s_An} of about 100 MHz (not shown in Fig. 8). Using Eq. (10) and taking the temperature as a parameter, we have calculated c_{11}, c_{13}, and c_{33}, which turn out to be positive in the temperature range investigated. The knowledge of the stiffness tensor enabled us to determine the polar plot of the quasilongitudinal [Fig. 16(a)] branch and an upper limit for the quasitransverse [Fig. 16(b)] branch of the hypersound velocity of the nematic state of 5O.8. As a result, we found that within the temperature regime where c_{11} slows down, the elastic moduli related to the quasitransverse sound velocity branch $v_{QT}(\varphi)$ became negative for angles $\varphi\in\,]0,\pi/2[$ (modulo $\pi/2$). Using the relation for the bulk modulus of materials with hexagonal symmetry [40]

$$K=\frac{(c_{11}c_{33}-c_{13}^2)}{(c_{11}+c_{33}-2c_{13})}\ , \tag{13}$$

we verified the stability condition $K(T)>0$ for the whole temperature range under study (Fig. 17). In addition, this figure shows the temperature dependence of the quantity $(c_{11}c_{33}-c_{13}^2)$. This quantity, which should be positive in order to have propagating QT modes, becomes negative near, but still above the nematic–smectic-A transition at $T\cong 336$ K. $(c_{11}c_{33}-c_{13}^2)\leq 0$ signifies that, provided the relation $[c_{11},c_{33},c_{13}]\gg c_{44}$ still holds true, the sound velocity $v_{QT}(\varphi)$ becomes imaginary, thus yielding an acoustic instability that ultimately prevents the propagation of QT modes. This acoustic instability of the QT mode occurs even if the attenuation of the quasishear mode is moderate. The origin of this instability is not yet clear.

The inset of Fig. 8 shows a second set of data for the nematic phase of 5O.8 which differs completely from the first. $v_1(T)$ and $v_3(T)$ of this second data set were obtained after cooling the liquid crystal only slightly into the smectic-A phase and then investigating the sample again up to T_{ni}. The softening of $c_{11}(T)$ has obviously disappeared. However, further measuring runs, which started in the smectic-B phase, reproduced the main data of Fig. 8 including the softening of c_{11}. It seems that cooling the sample to temperatures just below T_{s_An} creates a monotropic phase, from which the transition to the nematic state proceeds continuously or almost continuously.

Brillouin investigations have been performed at the

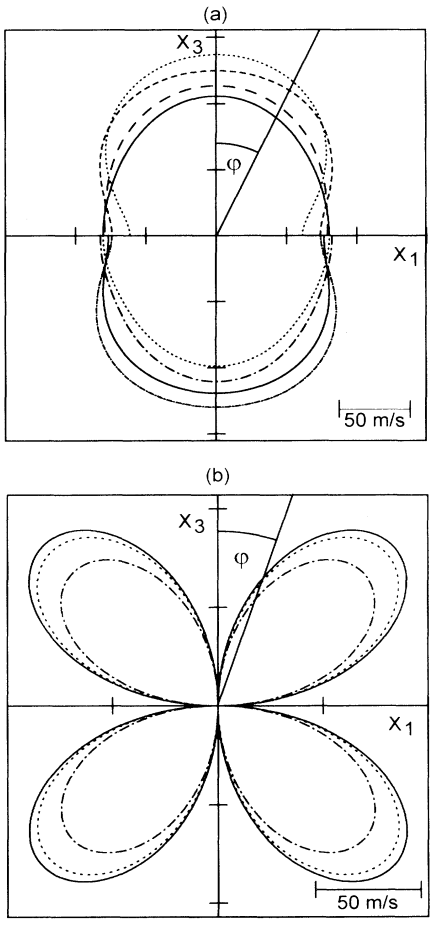

FIG. 16. Calculated sound velocity polar diagrams of the phonon branches of 5O.8 at various temperatures (for further information, see text). (a) Quasilongitudinal phonon branches (zero point suppression by 1300 m/s.). Upper half plane: . . . .: 341 K; - - - -: 342.8 K; — — —: 344.6 K; ——: 346.5 K. Lower half plane: . . . .: 347.4 K; — — —: 345.5 K; ——: 343.7 K; —.—.—.: 341.9 K. (b) Quasitransverse phonon branches; ——: 347.4 K; . . . .: 345.5 K; — — —: 346.5 K.

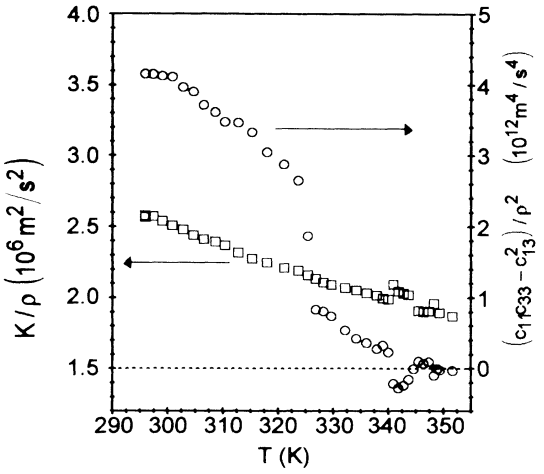

FIG. 17. Compression modulus K/ρ and $(c_{11}c_{33}-c_{13}^2)/\rho^2$ of 5O.8 as functions of temperature.

nematic–smectic-A phase transition of 8CB (Fig. 6) and at the nematic–smectic-A–smectic-B phase transitions of 5O.8 (Fig. 8). The hypersonic behavior is quite different for the two mesomorphic materials.

According to our hypersonic data for 8CB, the two principal longitudinal sound modes are not affected by the nematic–smectic-A transition at T_{s_An}. Within the margin of error the same holds true for the related attenuation coefficients Γ. From the hydrodynamic approach [4] it follows that in smectic phases an elastic anisotropy should be possible even in the hydrodynamic limit. However, for 8CB the additional broken translational symmetry does not affect the hypersonic anisotropy. This fact suggests that at least for 8CB the hypersonic anisotropy is, as it is in the nematic state, predominantly determined by the orientational molecular order and not influenced by the lamellar stacking.

The system 5O.8 exhibits both smectic-B and smectic-A phases. Figure 8 shows the temperature dependent sound velocity measured by Brillouin spectroscopy together with the ultrasonic results of Abed and Benguigui [34]. Again there is a difference between the absolute values of the sound velocities measured at ultrasonic and hypersonic frequencies. The hypersonic relaxation process discussed above seems to be active in the smectic-A as well as smectic-B phases. The longitudinal acoustic anisotropy of the smectic-A phase remains small but positive. At the smectic-A–smectic-B transition at $T_{s_As_B}$ this anisotropy undergoes an inversion running through an elastically isotropic state. However, even in the smectic-B phase the longitudinal anisotropies remain small, indicating a weak coupling between the order parameter and the longitudinal elastic strain at the frequencies involved as well as nearly purely longitudinal polarized QL modes. The anisotropy inversion at $T_{s_As_B}$ can be related to the onset of two-dimensional crystalline order within the smectic-B layers that also explains the overall increasing stiffness below the smectic-A–smectic-B transition (Fig. 8). A plane wave traveling perpendicular to the preferential direction only probes these crystalline molecular interactions, whereas a wave traveling along the preferential direction probes an elastic series connection of stiff layers and soft interlayer regions which in total yield the result $c_{33}<c_{11}$.

It is interesting to note that the compression modulus K of 5O.8 shown in Fig. 17 is not affected by the various phase transitions, which reflects the fact that, even at hypersonic frequencies, this modulus is predominantly determined by weak van der Waals interactions between the molecules. In contrast to the temperature behavior of the pure modes, the quasilongitudinal sound mode at $\varphi=45°$, $v_{\mathrm{QL}}(\varphi=45°,T)$, also remains unaffected at the various phase transitions, especially at the smectic-A–smectic-B transition. As the difference $c_{33}-c_{11}$ remains small in each phase, the latter observation is, according to Eqs. (10), (11), and (13), a direct consequence of the former. This conclusion only holds true if c_{66} is small compared to c_{11} [40]. Unfortunately, because of the small laser power allowed for these measurements (Sec. II), we detected neither the T nor the QT branch of the smectic-B phase of 5O.8. Taking $c_{66}=0.2$ GPa, reported by Liao, Clark, and Pershan [37] for β-methylbutyl-p[(p-methoxybenzylidene)amino] cinnamate as a reference, we can confirm our conclusion made above.

IV. CONCLUSIONS

Within this work we present results concerning the high-frequency second-order elastic properties of several classes of nematic liquid crystals including classical nematics and nematic glass formers. In contrast to ultrasonic experiments on classical liquid crystals, Brillouin experiments do not show any critical slowing down of the longitudinal polarized sound velocities around the nematic-isotropic phase transition, although hypersonic relaxation processes are active. Concerning order parameter fluctuations, the hypersonic velocity is measured in the slow motion regime. Generally, ultrasonic measurements on the mesomorphic as well as the isotropic states of classical liquid crystals yield lower absolute sound velocities than Brillouin experiments. Moreover, whereas ultrasonic measurements show no or nearly no sound velocity anisotropy in the nematic state, Brillouin experiments generally do. A qualitatively and quantitatively different hypersonic behavior, including the appearance of pure shear modes, was found for glass-forming nematics. From these findings we concluded that a dynamic glass transition is not responsible for the hypersonic properties of ncLC's. The acoustic properties of the latter class of materials are interpreted as a consequence of the continuation of a thermal relaxation process into the mesomorphic state, introduced for the isotropic state of liquid crystals earlier. The temperature behavior of the optoacoustical dispersion function $D^{90\mathrm{R}}$ supports the relaxation hypothesis. From the behavior of $D_1^{90\mathrm{R}}$ and $D_3^{90\mathrm{R}}$ in comparison with n_1 and n_3 in the nematic phases of 5CB and 6CB, we claim that the hypersonic relaxation mechanism is almost not renormalized at the nematic-isotropic transition. The universality of the process for

ncLC's is pointed out by the qualitative and quantitative similarity of the presented data for all investigated material classes. In connection with the appearance of hypersonic anisotropies in the nematic state, we determined the eigenvectors of quasilongitudinal modes in order to estimate whether the propagation of QT modes in nematics is detectable by high performance Brillouin spectroscopy or not. We present the example of 5O.8, where we found an acoustic instability within the nematic phase.

ACKNOWLEDGMENTS

We are indebted to Professor P. Martinoty for many discussions about the ultrasonic and relaxation aspects of the presented data. He also helped us much through critical reading, comments, and corrections of the manuscript. We would like to thank Professor D. Demus and Dr. W. Wedler for fruitful discussions about glass-forming nematics and for the supply of MIE2.

[1] P. G. De Gennes, *The Physics of Liquid Crystals* (Clarendon, Oxford, 1974).
[2] D. Forster, *Hydrodynamic Fluctuations, Broken Symmetries and Correlation Functions* (Benjamin, London, 1975).
[3] C. W. Oseen, Trans. Faraday Soc. **29**, 883 (1933); H. Zocher, *ibid.* **29**, 945 (1933); F. C. Frank, Discuss. Faraday Soc. **25**, 19 (1958).
[4] P. C. Martin, O. Parodi, and P. S. Pershan, Phys. Rev. A **6**, 2401 (1972).
[5] F. Jähnig, Z. Phys. **258**, 199 (1973).
[6] K. Miyano and J. B. Ketterson, in *Physical Acoustics,* edited by Thurston Mason (Academic, New York, 1979).
[7] S. Candau, P. Martinoty, and R. Zana, J. Phys. Lett. **36**, L13 (1975).
[8] N. A. Clark and Y. Liao, J. Chem. Phys. **63**, 4133 (1975).
[9] T. Harada and P. P. Crooker, Mol. Cryst. Liq. Cryst. **42**, 283 (1977).
[10] C. Grammes, J. K. Krüger, K.-P. Bohn, J. Baller, C. Fischer, C. Schorr, D. Rogez, and P. Alnot, Phys. Rev. E **51**, 430 (1995).
[11] G. W. Bradberry and J. M. Vaughan, Phys. Lett. **62A**, 225 (1977).
[12] G. W. Bradberry and C. F. Clarke, Phys. Lett. **95A**, 305 (1983).
[13] J. K. Krüger, in *Optical Techniques to Characterize Polymer Systems,* edited by H. Bässler (Elsevier, Amsterdam, 1989).
[14] C. Grammes, Ph.D. thesis, Saarbrücken, 1993.
[15] D. G. Gleed, J. R. Sambles, and G. W. Bradberry, Phys. Lett. A **134**, 440 (1989).
[16] J. K. Krüger, L. Peetz, R. Siems, H.-G. Unruh, M. Eich, O. Herrmann-Schönherr, and J. H. Wendorff, Phys. Rev. A **37**, 2637 (1988).
[17] J. K. Krüger, C. Grammes, and J. H. Wendorff, in *Dynamics of Disordered Materials,* edited by D. Richter *et al.*, Springer Proceedings in Physics Vol. 37 (Springer-Verlag, Berlin, 1989), p. 216.
[18] J. K. Krüger, C. Grammes, and J. H. Wendorff, Colloid Polym. Sci. **80**, 45 (1989).
[19] J. K. Krüger, A. Marx, L. Peetz, R. Roberts, and H.-G. Unruh, Colloid Polym. Sci. **264**, 403 (1986).
[20] J. K. Krüger, R. Kimmich, J. Sandercock, and H.-G. Unruh, Polym. Bull. **5**, 615 (1981).
[21] B. A. Auld, in *Acoustic Fields and Waves in Solids* (Wiley, New York, 1973).
[22] D. Collin, J. L. Gallani, and P. Martinoty, Phys. Rev. A **34**, 2255 (1986).
[23] W. Wedler and D. Demus were so kind to introduce us to the field of glass-forming nLC's and supply us with the material MIE2.
[24] W. Wedler, Ph.D. thesis, Halle, 1989.
[25] H. Kresse, S. Ernst, W. Wedler, D. Demus, and F. Kremer, Ber. Bunsenges. Phys. Chem. **94**, 1478 (1990).
[26] J. C. Wittmann and P. Smith, Nature **352**, 414 (1991).
[27] J. K. Krüger, M. Prechtl, P. Smith, S. Meyer, and J. C. Wittmann, J. Polym. Sci. B **30**, 1173 (1992).
[28] R. Jiménez, J. K. Krüger, M. Prechtl, C. Grammes, and P. Alnot, J. Phys. Condens. Matter **6**, 10 977 (1994).
[29] E. D. Liebermann, J. D. Lee, and F. C. Moon, Appl. Phys. Lett. **18**, 280 (1971).
[30] A. E. Lord and M. M. Labes, Phys. Rev. Lett. **25**, 570 (1970).
[31] F. Jähnig, Chem. Phys. Lett. **23**, 262 (1973).
[32] S. Nagai, P. Martinoty, S. Candau, and R. Zana, Mol. Cryst. Liq. Cryst. **31**, 243 (1975).
[33] V. Zwetkoff, Acta Physicochim. (USSR) **16**, 132 (1942).
[34] A. H. Abed and L. Benguigui, Liq. Cryst. **9**, 741 (1991).
[35] D. Eden, C. W. Garland, and R. C. Williamson, J. Chem. Phys. **58**, 1861 (1973).
[36] P. P. Karat and N. V. Madhusudana, Mol. Cryst. Liq. Cryst. **36**, 51 (1976).
[37] Y. Liao, A. Clark, and P. S. Pershan, Phys. Rev. Lett. **30**, 639 (1973).
[38] J. K. Krüger, R. Jiménez, K.-P. Bohn, J. Petersson, J. Albers, A. Klöpperpieper, E. Sauerland, and H.-E. Müser, Phys. Rev. B **42**, 8537 (1990).
[39] A. Marx, J. K. Krüger, and H.-G. Unruh, Z. Phys. B **75**, 101 (1989).
[40] G. Grimvall, *Thermophysical Properties of Materials* (North-Holland, Amsterdam, 1986).